Broad SARS-CoV-2 cell tropism and immunopathology in lung tissues from fatal COVID-19

Suzane Ramos da Silva,[1,a] Enguo Ju,[1,a] Wen Meng,[1] Alberto E. Paniz Mondolfi [2] Sanja Dacic,[3] Anthony Green,[4] Clare Bryce,[2] Zachary Grimes,[2] Mary Fowkes,[2] Emilia M. Sordillo,[2] Carlos Cordon-Cardo,[2] Haitao Guo,[1] Shou-Jiang Gao[1]

[1]Cancer Virology Program, UPMC Hillman Cancer Center and Department of Microbiology and Molecular Genetics, University of Pittsburgh School of Medicine, Pittsburgh, Pennsylvania, USA, [2]Department of Pathology, Molecular and Cell-Based Medicine, Icahn School of Medicine at Mount Sinai, New York, New York, USA, [3]Department of Pathology, University of Pittsburgh School of Medicine, Pittsburgh, Pennsylvania, USA, [4]Tissue and Research Pathology Core, UPMC Hillman Cancer Center, University of Pittsburgh School of Medicine, Pittsburgh, Pennsylvania, USA.

[a]S.R.S. and E.J. contributed equally to this work.

Correspondence: Prof S.-J. Gao, Cancer Virology Program, UPMC Hillman Cancer Center and Department of Microbiology and Molecular Genetics, University of Pittsburgh School of Medicine, Pittsburgh, Pennsylvania, USA (gaos8@upmc.edu)

Abstract

Background. COVID-19 patients manifest with pulmonary symptoms reflected by diffuse alveolar damage (DAD), excessive inflammation, and thromboembolism. The mechanisms mediating these processes remain unclear.

Methods. We performed multicolor staining for SARS-CoV-2 proteins and lineage markers to define viral tropism and lung pathobiology in 5 autopsy cases.

Results. Lung parenchyma showed severe DAD with thromboemboli. Viral infection was found in an extensive range of cells including pneumocyte type II, ciliated, goblet, club-like and endothelial cells. Over 90% infiltrating immune cells were positive for viral proteins including macrophages, monocytes, neutrophils, and natural killer (NK), B and T cells. Most but not all infected cells were ACE2-positive. The numbers of infected and ACE2-positive cells are associated with extensive tissue damage. Infected tissues exhibited high inflammatory cells including macrophages, monocytes, neutrophils and NK cells, and low B- but abundant T-cells consisting of mainly T helper cells, few cytotoxic T cells, and no T regulatory cell. Robust interleukin-6 expression was present in most cells, with or without infection.

Conclusions. In fatal COVID-19 lungs, there are broad SARS-CoV-2 cell tropisms, extensive infiltrated innate immune cells, and activation and depletion of adaptive immune cells, contributing to severe tissue damage, thromboemboli, excess inflammation and compromised immune responses.

Keywords. SARS-CoV-2; COVID-19; cell tropism; diffuse alveolar damage; thromboemboli; IL6; inflammation; immunosuppression; immunofluorescence assay; immunohistochemistry

.

Highlights

We provide an atlas of lung immunopathology of fatal SARS-CoV-2 infections, revealing:

- Unexpected broad cell tropism and infection of parenchymal, endothelial and immune cells by SARS-CoV-2, which are associated with massive tissue damage and thromboemboli;
- Extensive infiltration and activation of immune cells, and suppression of B cells and cytotoxic T cells;
- Pronounced IL6 expression in all types of infected and uninfected cells.

INTRODUCTION

Coronavirus Disease 2019 (COVID-19) is a complex disease caused by Severe Acute Respiratory Syndrome Coronavirus-2 (SARS-CoV-2) infection[1]. Multiple organs are affected, and severe lung damage is a prominent finding in fatal cases[2, 3]. Although dysregulated immune responses and excess inflammation are commonly observed in lung tissues from these patients, the precise mechanism underlying the pulmonary pathology remains unclear.

Single cell RNA sequencing (scRNA-seq) analysis of lung tissues from healthy subjects have revealed that many cell types express SARS-CoV-2 entry receptors and cofactors, including angiotensin-converting enzyme-2 (ACE2), transmembrane serine protease 2 (TMPRSS2), and furin, suggesting susceptibility of these cells to infection[4-7]. Furthermore, scRNA-seq analysis of bronchoalveolar lavage fluid, blood, oropharyngeal or lung tissues from COVID-19 patients has identified different types of SARS-CoV-2-infected cells, including macrophages, neutrophils, type II pneumocytes (AT2), and ciliated and endothelial cells[8-10]. However, in general, these studies detected low numbers of infected cells, which harbored low counts of viral genomes and transcripts[8-10]. The reason for the discrepancy between high numbers of cells expressing viral entry receptors/cofactors and low numbers of infected cells even in COVID-19 patients with severe pulmonary disease remains unclear. Interestingly, the expression of ACE2, TMPRSS2 and furin is upregulated in macrophages, neutrophils, AT2 and ciliated cells in COVID-19 patients compared to healthy controls, and that type 1 interferons (IFNs) induce the expression of ACE2 in epithelial cells, hence increasing their susceptibility to infection[11]. However, another study showed that type 1 IFNs only induced an ACE variant expression but not ACE2 involved in viral entry[12]. Although immunohistochemistry (IHC) staining of lung tissues detected SARS-CoV-2 spike (S1) or nucleocapsid (NC) protein in macrophages ($CD68^+$ and $CD183^+$), and AT2, ciliated, goblet, club and endothelial progenitor cells, infected cells were often observed at low numbers, and the exact identity of many infected cells remain unknown[13-

15]. Questions remain regarding the SARS-CoV-2 targeted cell types and percentages of infected cells, and whether the extent of infection is correlated with expression of viral entry factors and disease status.

Interleukin-6 (IL6), among others including IL1β, IL10, tumor necrosis factor-α (TNF-α), granulocyte-macrophage colony-stimulating factor (GM-CSF), IFN-γ-induced protein 10 (IP10), IL17, and IL1 receptor antagonist (IL1RA), is one of the most abundant cytokines detected in patients with severe COVID-19, and its expression is correlated with patient prognosis[16-20]. Although treatments with IL6 antagonists have been shown to improve the survival and shortened the recovery time[21, 22], other studies argued that IL6 is beneficial for infection[23, 24]. The cell types responsible for the increased IL6 expression in the lungs are poorly defined, and consequently the relationship between IL6 expression and the extent of SARS-CoV-2 infection, as well as disease severity has not been clearly defined.

We found broad SARS-CoV-2 infection in lungs of these patients, and more infected cells were observed in cases with more extensive pathology. Infected immune cell types were comprised of monocytes and macrophages ($CD68^+$ or $CD163^+$), neutrophils ($ELA\text{-}2^+$), and natural killer (NK) ($CD56^+$), B ($CD20^+$), and T ($CD3\varepsilon^+$, $CD4^+$and $CD8^+$) cells, including activated B and T ($HLA\text{-}DR^+$) cells. We directly visualized by IHC and immunofluorescence staining (IF) of SARS-CoV-2 infection of neutrophils and different T cell subtypes, and simultaneously detected SARS-CoV-2 infection and ACE2 expression in AT2 pneumocytes, and club-like, goblet and endothelial cells. Finally, we found wide spread IL6 expression in lung parenchyma involving most cells and cell types regardless of individual cell infection status.

MATERIALS AND METHODS

COVID-19 lung tissue samples

Anonymized postmortem specimens were collected from five adults (4 male and 1 female) with fatal SARS-CoV-2 infection by the Autopsy Service of the Department of Pathology, Molecular and Cell-based Medicine at the Icahn School of Medicine at Mount Sinai. All patients were admitted because of symptomatic COVID-19 and a positive nasopharyngeal swab test for SARS-CoV-2 by real-time reverse-transcription polymerase-chain-reaction amplification (RT-PCR, cobas® 6800 system, RocheDiagnostics). Clinical-pathologic findings are summarized in Table 1. Autopsies were performed with written consent from the legal next-of-kin, and specimens were obtained per the Autopsy Service protocol.

Lung tissue samples from subjects with other lung conditions

Anonymized lung specimens from five adults with other lung conditions but without COVID-19 were used as controls. Clinical-pathologic findings are summarized in Supplementary Table 1.

Study approval

Specimens obtained at autopsy do not meet the definition of a living individual per Federal Regulations 45 CFR 46.102, and as such, research using specimens obtained at autopsy does not meet the requirements for Institutional Review Board (IRB) review or oversight under the Icahn School of Medicine Program for the Protection of Human Subjects. The University of Pittsburgh IRB determined that the study is not research involving human

subjects as defined by DHHS and FDA regulations and waived of ethical oversight (STUDY20050085).

Hematoxylin-eosin staining, immunohistochemistry, and immunofluorescence assay

We analyzed the expression of S1 and NC in postmortem lung tissues from five fatal COVID-19 patients. We performed multicolor IF for SARS-CoV-2 proteins, ACE2 protein and lineage-restricted cell markers. Postmortem biopsies were fixed with 10% neutral buffered formalin and embedded in paraffin. Slides were stained with H&E for histological analyses. For IHC single staining (CD3, CD4, CD8, CD45, CD19, CD20 and FOXP3), the slides were deparaffinized at 60ºC for 30 min and rehydrated using a standard histology protocol of 3 changes of xylene of 5 min each followed by 3 changes of 100% ethanol, 2 with 95% ethanol and 1 with 70% ethanol for 1 min each, then rinsed in distilled water. Antigen retrieval was performed using citrate buffer (Agilent Dako, Santa Clara, CA, USA) in Decloaking chamber at 123°C for 2 min. The slides were stained using an Autostainer Plus (Agilent Dako) platform with TBS-T rinse buffer (Agilent Dako). The IHC slides were treated with 3% hydrogen peroxide for 10 min. The primary antibodies were applied at room temperature for 30 min, followed by 30 min of secondary antibodies Envision + Dual Link (Agilent Dako) HRP polymer at room temperature. Slides were exposed to 3,3, Diaminobenzidine+ (Agilent Dako) for 5 min, and counterstained with Hematoxylin (Agilent Dako).

For IF, slides were deparaffinized at 95°C for 10 min, followed by 3 washes of xylene for 5 min. Dehydration was performed with step-wise 10 min incubation of ethanol at 100%, 95% and 75%, followed by water. Antigen retrieval used citrate buffer at pH 6.0 on microwave for 3 min at maximum potency, followed by 15 min with 30% potency, and cooled down for 30 min at room temperature. Slides were treated for 1 h with 5% bovine serum albumin (BSA) solution. Primary antibodies were incubated overnight at 4°C, and secondary

antibodies were incubated for 1 h at room temperature. Slides were treated with Vector TrueVIEW™ autofluorescence quenching (Vector Laboratories, Burlingame, CA, USA) for 5 min followed by incubation with 4',6-diamidino-2-phenylindole (DAPI) for 10 min.

Supplementary Table 2 summarizes all antibodies and dilutions used in the study.

RESULTS

Histologic findings

Lung tissues from all five cases showed various combinations of diffuse alveolar damage (DAD), pulmonary thromboemboli and pulmonary consolidation (Figure 1A, Table 1 and Supplementary Figure 1A). Case 4 had the most extensive and severe pathologic changes, including early exudative phase of DAD, vascular congestion and rare hyaline membranes. Air-spaces filled with blood were noted in cases 1, 2 and 4. The least dramatic changes were cases 2 and 3; both had incidental anthracosis. These findings are consistent with previous descriptions of lung pathology in COVID-19 patients[25-28].

Detection of broad SARS-CoV-2 infection and ACE2 protein expression

Evidence of SARS-CoV-2 infection was detected by IHC with antibodies against the S1 protein receptor binding domain (RBD) and NC protein. All 5 cases were positive for S1 and NC proteins (Figure 1B and Supplementary Figure 1B) with the widest distribution of infected cells observed in case 4 followed by cases 1 and 5. The fewest infected cells were observed in cases 2 and 3. Tissue damage was widespread in all cases. Case 5 had the most structurally preserved specimen with infected cells present in patches, rather than throughout the specimen. ACE2 protein was widely detected in different cell types in all cases including immune cells comprised of monocytes, macrophages, neutrophils and

lymphocytes (Figure 1C and Supplementary Figure 1C). The extent of ACE2 protein expression correlated with that of SARS-CoV-2 infection with cases 2 and 3 having the lowest numbers of cells expressing ACE2 protein (Supplementary Figure 1C). Control lung tissues from 5 subjects without COVID-19 had similar ACE2 staining pattern but none had any positive staining for S1 and NC proteins (Supplementary Figure 2A-C).

Detection of abundant innate immune response cells and low numbers of adaptive immune cells

Infiltration of immune cells is a common sequel to infection. We identified immune cells by staining for cell markers by IHC (Supplementary Figure 3). Cells positive for CD45 (leukocyte common antigen, LCA), a marker for most hematopoietic cells, were more abundant in COVID-19 cases compared to controls (Figure 1D and Supplementary Figure 4C, 5C). Increased infiltrating monocytes and macrophages were detected in COVID-19 cases compared to controls using CD68 as a monocyte, pan-macrophage or M1 marker, and CD163 as a M2 cell marker (Figure 1D and Supplementary Figure 4A, 5A). $CD68^+$ cells were more abundant than $CD163^+$ cells in COVID-19 cases.

We identified B cells by staining for CD19 and CD20. Almost no B cells were detected in controls (Supplementary Figure 5B). However, a few $CD19^+$ cells were detected in COVID-19 tissues, and cases 1 and 2 showed pockets of infiltrating $CD20^+$ cells, which appeared to be surrounding venous structures (Figure 1D and Supplementary Figure 4B). Infiltration by T cell receptor (TCR) $CD3\varepsilon^+$ cells, predominantly T $CD4^+$ helper, and fewer T $CD8^+$ cytotoxic cells, was detected in COVID-19 cases but with no obvious difference from controls (Figure 1D and Supplementary Figure 4C, 5C). Both control and COVID-19 tissues were negative for FOXP3, a marker for natural T regulatory (Treg) cells (Figure 1D and Supplementary Figure 4C, 5C).

Most SARS-CoV-2-infected cells have detectable ACE2 protein expression

Since ACE2 protein expression was correlated with SARS-CoV-2 infection (Figure 1B, C and Supplementary Figure 1B, C), we performed dual IF staining for ACE2 and S1 protein (Figure 2A and Supplementary Figure 6). Most of the infected cells had ACE2 protein expression but some ACE2-negative infected cells were also observed which could be due to low ACE2 protein level outside the detection range, downregulation of ACE2 protein expression at some stage(s) of SARS-CoV-2 infection, virus cell-to-cell spread, or presence of an alternative SARS-CoV-2 receptor. Consistent with our IHC findings, cases displaying a broader range of SARS-CoV-2-infected cell types also had more ACE2-positive cells (Supplementary Figure 6). Cases 2 and 3 had the lowest numbers of ACE2-positive cells and the least infected cells.

SARS-CoV-2 infects most parenchymal cell lineages in lung tissues

Since we observed extensive damage to lung tissues (Figure 1A and Supplementary Figure 1A), we performed triple-color staining for SARS-CoV-2 and ACE2 proteins in lung parenchymal cells including AT2 cells, ciliated cells (tyr-α-tubulin), goblet cells (MUC5AC), and club-like cells (MUC5B) (Figure 2B-E and Supplementary Figure 7). AT2 cells, a major target of SARS-CoV-2 infection in lung tissues[7], were positive for ACE2 and S1 proteins (Figure 2B and Supplementary Figure 7A). AT2 cells were identified using an anti-HT2-280 mouse IgM monoclonal antibody specific to human lung alveolar type 2 cells. Intact cell membranes and less extensive infection by SARS-CoV-2 were observed for cases 2 and 3 while there were more extensive infection of AT2 cells along with ruptured cell membranes, possibly related to viral shedding in case 4 (Supplementary Figure 7A).

Tyr-α-tubulin was used as a microtubule marker for identifying ciliated cells among others. SARS-CoV-2 extensively infected cells expressing tyr-α-tubulin including ciliated cells identified by their morphology in all cases (Figure 2C and Supplementary Figure 7B).

The predominant mucins expressed in the lung are MUC5AC, mainly found in goblet cells, and MUC5B, mostly expressed in club-like cells. Both MUC5AC$^+$ and MUC5B$^+$ cells were infected by SARS-CoV-2 and expressed ACE2 (Figure 2D, E and Supplementary Figure 7C, D). MUC5B$^+$ cells were more abundant than MUC5AC$^+$ cells.

SARS-CoV-2 infects small number of vascular endothelial cells in lung tissues from COVID-19 patients[29]. We observed extensive SARS-CoV-2 infection and damage in CD34$^+$ or CD31$^+$ endothelial cells (Figure 2F, G and Supplementary Figure 8), which might be the cause of widespread microhemorrhages and infarction observed in these tissues.

SARS-CoV-2 infects macrophages, neutrophils and NK cells in lung tissues

Since we detected vast infiltrations by innate immune response cells, we examined SARS-CoV-2 infection in these cells. Monocytes and macrophages (CD68$^+$ or CD163$^+$) were widely infected by SARS-CoV-2 (Figure 3A, B, E and Supplementary Figure 9A, B). Neutrophils, positive for elastase-2 (ELA-2$^+$) protein, were extensively infected by SARS-CoV-2 (Figure 3C, E and Supplementary Figure 9C). The extent of neutrophil infection was positively correlated with ACE2 protein expression in all cases except for case 5, for which 96% of cells expressed ACE2, but only 19% had detectable S1 protein (Figure 3E). We detected S1 protein in NK cells (CD56$^+$) (Figure 3D and Supplementary Figure 9D); however the percentages of infected cells were much smaller than other cell types examined, ranging from 0 to 40% (Figure 3E).

Broad infection of adaptive immune cells by SARS-CoV-2 in lung tissues

Among the adaptive immune cells, B cells (CD20$^+$) were found in low numbers in the lung specimens, but ACE2 protein expression and SARS-CoV-2 infection were positively correlated in these cells (Figure 4A, F and Supplementary Figure 10). Different types of T-

cells expressing CD4 (Figure 4B, F and Supplementary Figure 11A), CD8 (Figure 4C, F and Supplementary Figure 11B) and CD3ε (Figure 4D, F and Supplementary Figure 11C) were all co-stained with NC protein. Furthermore, HLA-DR, a marker of activated B and T cells, co-stained with NC protein (Figure 4E, F and Supplementary Figure 11D). Interestingly, $CD4^+$, $CD8^+$ or $CD3\varepsilon^+$ T cells presented either as a membrane-associated pattern or as a dot-like organization pattern, possibly as the result of membrane rupture following SARS-CoV-2 infection (Supplementary Figure 11E).

Detection of SARS-CoV-2 proteins not associated with virions in lung cells

To exclude the possibility that the detection of S1 and NC proteins in different cells were not due to any unspecific events such as engulfment, we stained for NSP8 and NSP13 proteins. Both proteins are not associated with virions and expressed only during viral replication. Indeed, we detected wide expression of both proteins in COVID-19 cases with NSP8 being more abundant than NSP13 protein (Supplementary Figure 12). Dual staining with CD68 revealed NSP8 and NSP13 expression in monocytes and macrophages. These results provided clear evidence of SARS-CoV-2 replication in these lung tissues.

IL6 is widely detected in both SARS-CoV-2-infected and uninfected cells

IL6 is one of the most abundant cytokines detected in COVID-19 patients and its level is correlated with prognosis[16, 20-22]. Upregulation of IL6 in lungs of COVID-19 patients have been reported[30]. In all cases, we found IL6 expression in most cells examined, with or without SARS-CoV-2 infection (Figure 5A and Supplementary Figure 13). Tissue regions with higher numbers of infected cells also had more cells expressing IL-6 (Supplementary Figure 13). Compared to controls, COVID-19 cases generally had higher numbers of IL6-positive cells albeit strong staining in some areas was observed with control 2, which could

be due to its specific lung condition (Supplementary Figure 13, 14). Dual staining of IL6 and CD20, CD68 or CD163 in COVID-19 cases revealed that B cells, monocytes and macrophages were strongly positive for IL6 (Figure 5B).

DISCUSSION

Respiratory symptoms are a prominent complaint during most SARS-CoV-2 infections, and progressive respiratory dysfunction is a major feature of fatal COVID-19[1, 3]. Our results present a direct visualization of multiple cell types infected by SARS-CoV-2 from patients who died of COVID-19, and offer insights into the pathogenesis of the overwhelming damage found in lung tissues.

The detection of S1 or NC protein revealed widespread SARS-CoV-2 infection in lung tissues, including multiple lung parenchymal cell types and multiple cell types involved in immune responses. These viral proteins were most abundant in specimens with the most histologic evidence of tissue damage. As expected, the extent of infection was positively correlated with ACE2-positive cells numbers. However, we also found SARS-CoV-2 infection in ACE2-negative cells, supporting a role for other possible receptors for viral entry into ACE-negative cells. It is important to note that there may be multiple factors that might influence ACE2 expression during SARS-CoV-2 infection and should be considered as confounders. For example, ACE2 expression can be stimulated by IFNs[7, 11]. Furthermore, ACE2 may have a role in protection against severe acute lung failure, as has been reported in severe COVID-19 patients[31].

We obtained direct evidence for widespread ACE2 expression and extensive SARS-CoV-2 infection among different cell types using multicolor IF staining for SARS-CoV-2 and ACE2 proteins in different pulmonary parenchymal and immune cells. Among lung parenchymal cells that were both ACE2-positive and SARS-CoV-2-infected included AT2 (HT2-280), ciliated (Tyr-α-tubulin), goblet (MUC5AC), club-like (MUC5B) and vascular

endothelial cells ($CD31^+$ or $CD34^+$). Our findings are consistent with studies showing SARS-CoV-2 infection of ciliated, goblet and club cells by RNA-*in situ* hybridization (ISH)[32]; and pneumocytes, ciliated, secretory and lymphomononuclear cells by IHC[15] in lung tissues from COVID-19 patients. In *ex-vivo* culture, SARS-CoV-2 infects type I pneumocytes, ciliated, goblet and club cells as well as conjunctival mucosa[14].

We detected ACE2 protein expression in different immune cells including $CD68^+$ and $CD163^+$ monocytes and macrophages, $ELA\text{-}2^+$ neutrophils, $CD56^+$ NK cells, and B- and T-cells; these findings are consistent with previous reports based on scRNA-seq studies[4, 6, 7, 33]. ACE2 expression detected by flow cytometry in T cells from lung tissues from COVID-19 patients has been reported[34]. Notably, we found rates of SARS-CoV-2 infection approaching 100% for most types of immune cells, in contrast to a much lower infection rate in NK cells (Figure 3E, 4F). Although SARS-CoV-2 proteins have been detected in macrophages by IHC[35], to our knowledge, our study is the first to demonstrate and quantify SARS-CoV-2 infection in different types of T cells and also in neutrophils. Our observation of SARS-CoV-2 infection of neutrophils was in contrast to the results of a study, which failed to detect any infected neutrophils[34]. The observed immune responses in lungs of fatal COVID-19 patients are different from acute infection of respiratory syncytial virus, which has strong neutrophil response positively correlated with disease severity and mediated by IL8, dendritic cells migration to lungs as the primary antigen-presenting cells, and an initial systemic T-cell lymphopenia followed by a pulmonary CD8+ T-cell response to mediate viral clearance[36].

We simultaneously identified SARS-CoV-2-infected and ACE2-expressing cells in parenchymal and immune cells in lung tissues from COVID-19 patients by multicolor staining. Infiltration and infection of immune cells such as macrophages are suggested as critical steps in the spread of SARS-CoV-2 infection to other organs[37] and in the initiation of uncontrolled inflammatory responses[38]. Furthermore, we observed SARS-CoV-2 infection and damage of vascular endothelial cells together with the vast inflammatory

infiltrations. These evidences of endothelitis and direct viral injury suggest that endothelial cell dysfunction plays an important role in the genesis of thromboembolic events in SARS-CoV-2 infection.

SARS-CoV-2 infection caused compromised immune response by dysregulating recruitment of immune cells[39]. Decreased levels of $CD4^+$ and $CD8^+$ T cells were associated with worsening COVID-19 outcomes[39, 40], and there was evidence of activation of $CD8^+$ T and NK cells as well as depletion of T cells in the lung tissues from COVID-19 patients[41-43], all of which could contribute to the increased proinflammatory or anti-inflammatory cytokines. We found that these immune cells were effectively infected by SARS-CoV-2, and noted a low level of $CD20^+$ B-cells, and a lower level of $CD8^+$ T as compared to $CD4^+$ T cells. These results suggested immunosuppression in the lungs of COVID-19 patients. Most of the inflammatory infiltrates were characterized as $CD68^+$, $CD163^+$ and $CD45^+$ cells. We did not detect an increase of $FOXP3^+$ Treg cells, which potentially support the T cell exhaustion theory[41-43], and the lack of Treg cells as a mechanism leading to failed control of excess inflammation observed in COVID-19 patients.

The inflammatory cytokine IL6 is highly expressed in COVID-19 patients, and an elevated IL6 level is associated with poor prognosis[16, 20-22]. However, the source of IL6 in COVID-19 patients remains unclear. We detected a broad, increased IL6 expression in all cell types in the lung specimens from all the cases. Furthermore, IL6 expression was associated with the detection of SARS-CoV-2 proteins, as well as with the degree of tissue damage. Of note, our findings were consistent with previous studies reporting that patients with a high level of IL6 and a poor prognosis also had decreased $CD8^+$ T, NK and Treg cells[41].

In summary, we performed a systematic analysis of SARS-CoV-2 infection in lung tissues from patients with fatal COVID-19, providing an atlas of lung immunopathology of the disease. We found a broad tropism of SARS-CoV-2 infection in pulmonary parenchymal and immune cells. Finally, we observed evidence of activation of immune cells, and possible depletion of B- and T-cells, potentially contributing to the failure of adaptive immune responses and excess inflammation. Further studies are required to delineate the mechanisms of SARS-CoV-2-triggered chemoattraction and immune exhaustion in the lungs of COVID-19 patients.

Notes

Acknowledgments. We thank Drs. Yuan Chang and Patrick Moore for their insightful comments and suggestions, Elaine V. Byrnes and Paul Knizner in the Pitt Biospecimen Core for the technical support.

Author Contributions. S.R.D.S. and E.G.J. contributed equally to this work. S.J.G. conceived and managed the project, and designed the study. S.R.D.S., E.G.J. and W.M. designed and performed the experiments. A.E.P.M., C.B., Z.G., M.F., E.M.S. and C.C.C. collected clinical specimens and data. S.D. examined immunohistochemistry results. A.G. carried out part of immunohistochemistry. S.R.D.S., E.G.J., W.M., HG and S.J.G. contributed to data interpretation. S.R.D.S. and S.J.G. wrote the first draft of the manuscript. All authors critically reviewed the manuscript, and approved the final manuscript for submission.

Disclaimer. The funding sources had no role in the study design, data collection, analysis, interpretation, or writing of the report.

Financial support. This study was supported by UPMC Hillman Cancer Center Startup Fund and Pittsburgh Foundation Endowed Chair in Drug Development for Immunotherapy (to SJG). This work used the UPMC Hillman Cancer Center and Tissue and Research Pathology/Pitt Biospecimen Core shared resource, which is supported in part by award P30CA047904.

Potential conflict of interests. S.D. reports personal fees from Astra Zeneca, Takeda and Bayer outside the submitted work. H.G. reports personal fees from Assembly Biosciences, grants and personal fees from Aligos Therapeutics, grants from Arbutus Biopharma, grants and personal fees from Spring Bank Pharmaceuticals, and grants from Zymeron Corporation outside the submitted work. In addition, H.G. has a patent US Patent No. 9657013 with royalties paid to Arbutus Biopharma, a patent US Patent No. 10072047 with royalties paid to Arbutus Biopharma, and a patent PCT/US2014/071555 pending outside the submitted work. All other authors declare no conflict of interest. All authors have submitted the ICMJE Form for Disclosure of Potential Conflicts of Interest.

References

1. Zhou P, Yang XL, Wang XG, Hu B, et al. A pneumonia outbreak associated with a new coronavirus of probable bat origin. Nature **2020;** 579:270-3.
2. Bryce C, Grimes Z, Pujadas E, Ahuja S, et al. Pathophysiology of SARS-CoV-2: targeting of endothelial cells renders a complex disease with thrombotic microangiopathy and aberrant immune response. The Mount Sinai COVID-19 autopsy experience. medRxiv **2020;** Posted May 22, 2020.
3. Xu Z, Shi L, Wang Y, Zhang J, et al. Pathological findings of COVID-19 associated with acute respiratory distress syndrome. Lancet Respir Med **2020;** 8:420-2.
4. Singh M, Bansal V, Feschotte C. A Single-Cell RNA Expression Map of Human Coronavirus Entry Factors. Cell Rep **2020;** 32:108175.
5. Travaglini KJ, Nabhan AN, Penland L, Sinha R, et al. A molecular cell atlas of the human lung from single-cell RNA sequencing. Nature **2020;** 587:619-25.
6. Qin S, Li W, Shi X, Wu Y, et al. 3044 Cases reveal important prognosis signatures of COVID-19 patients. Comput Struct Biotechnol J **2021;** 19:1163-75.
7. Ziegler CGK, Allon SJ, Nyquist SK, Mbano IM, et al. SARS-CoV-2 Receptor ACE2 Is an Interferon-Stimulated Gene in Human Airway Epithelial Cells and Is Detected in Specific Cell Subsets across Tissues. Cell **2020;** 181:1016-35 e19.
8. Bost P, Giladi A, Liu Y, Bendjelal Y, et al. Host-Viral Infection Maps Reveal Signatures of Severe COVID-19 Patients. Cell **2020;** 181:1475-88 e12.
9. Chua RL, Lukassen S, Trump S, Hennig BP, et al. COVID-19 severity correlates with airway epithelium-immune cell interactions identified by single-cell analysis. Nat Biotechnol **2020;** 38:970-9.
10. Liao M, Liu Y, Yuan J, Wen Y, et al. Single-cell landscape of bronchoalveolar immune cells in patients with COVID-19. Nat Med **2020;** 26:842-4.
11. Zhuang MW, Cheng Y, Zhang J, Jiang XM, et al. Increasing host cellular receptor-angiotensin-converting enzyme 2 expression by coronavirus may facilitate 2019-nCoV (or SARS-CoV-2) infection. J Med Virol **2020;** 92:2693-701.
12. Onabajo OO, Banday AR, Stanifer ML, Yan W, et al. Interferons and viruses induce a novel truncated ACE2 isoform and not the full-length SARS-CoV-2 receptor. Nat Genet **2020;** 52:1283-93.
13. Best Rocha A, Stroberg E, Barton LM, Duval EJ, et al. Detection of SARS-CoV-2 in formalin-fixed paraffin-embedded tissue sections using commercially available reagents. Lab Invest **2020**.
14. Hui KPY, Cheung MC, Perera R, Ng KC, et al. Tropism, replication competence, and innate immune responses of the coronavirus SARS-CoV-2 in human respiratory tract and conjunctiva: an analysis in ex-vivo and in-vitro cultures. Lancet Respir Med **2020;** 8:687-95.

15. Schaefer IM, Padera RF, Solomon IH, Kanjilal S, et al. In situ detection of SARS-CoV-2 in lungs and airways of patients with COVID-19. Mod Pathol **2020**.

16. Han H, Ma Q, Li C, Liu R, et al. Profiling serum cytokines in COVID-19 patients reveals IL-6 and IL-10 are disease severity predictors. Emerg Microbes Infect **2020;** 9:1123-30.

17. Wang J, Jiang M, Chen X, Montaner LJ. Cytokine storm and leukocyte changes in mild versus severe SARS-CoV-2 infection: Review of 3939 COVID-19 patients in China and emerging pathogenesis and therapy concepts. J Leukoc Biol **2020;** 108:17-41.

18. Chen X, Zhao B, Qu Y, Chen Y, et al. Detectable Serum Severe Acute Respiratory Syndrome Coronavirus 2 Viral Load (RNAemia) Is Closely Correlated With Drastically Elevated Interleukin 6 Level in Critically Ill Patients With Coronavirus Disease 2019. Clin Infect Dis **2020;** 71:1937-42.

19. Liu T, Zhang J, Yang Y, Ma H, et al. The role of interleukin-6 in monitoring severe case of coronavirus disease 2019. EMBO Mol Med **2020;** 12:e12421.

20. Aziz M, Fatima R, Assaly R. Elevated interleukin-6 and severe COVID-19: A meta-analysis. J Med Virol **2020**.

21. Eimer J, Vesterbacka J, Svensson AK, Stojanovic B, et al. Tocilizumab shortens time on mechanical ventilation and length of hospital stay in patients with severe COVID-19: a retrospective cohort study. J Intern Med **2020**.

22. Luo P, Liu Y, Qiu L, Liu X, et al. Tocilizumab treatment in COVID-19: A single center experience Journal of Medical Virology **2020;** 92:814-8.

23. Jamilloux Y, Henry T, Belot A, Viel S, et al. Should we stimulate or suppress immune responses in COVID-19? Cytokine and anti-cytokine interventions. Autoimmun Rev **2020;** 19:102567.

24. Scherger S, Henao-Martinez A, Franco-Paredes C, Shapiro L. Rethinking interleukin-6 blockade for treatment of COVID-19. Med Hypotheses **2020;** 144:110053.

25. Hariri LP, North CM, Shih AR, Israel RA, et al. Lung Histopathology in Coronavirus Disease 2019 as Compared With Severe Acute Respiratory Sydrome and H1N1 Influenza: A Systematic Review. Chest **2021;** 159:73-84.

26. Ackermann M, Verleden SE, Kuehnel M, Haverich A, et al. Pulmonary Vascular Endothelialitis, Thrombosis, and Angiogenesis in Covid-19. N Engl J Med **2020;** 383:120-8.

27. Fox SE, Akmatbekov A, Harbert JL, Li G, et al. Pulmonary and cardiac pathology in African American patients with COVID-19: an autopsy series from New Orleans. Lancet Respir Med **2020;** 8:681-6.

28. Borczuk AC, Salvatore SP, Seshan SV, Patel SS, et al. COVID-19 pulmonary pathology: a multi-institutional autopsy cohort from Italy and New York City. Mod Pathol **2020;** 33:2156-68.

29. Carnevale S, Beretta P, Morbini P. Direct endothelial damage and vasculitis due to SARS-CoV-2 in small bowel submucosa of COVID-19 patient with

diarrhea. Journal of Medical Virology **2020;** 2020 Jun 3:10.1002/jmv.26119. doi: 10.1002/jmv.26119.

30. Leng L, Cao R, Ma J, Mou D, et al. Pathological features of COVID-19-associated lung injury: a preliminary proteomics report based on clinical samples. Signal Transduct Target Ther **2020;** 5:240.
31. Imai Y, Kuba K, Rao S, Huan Y, et al. Angiotensin-converting enzyme 2 protects from severe acute lung failure. Nature **2005;** 436:112-6.
32. Hou YJ, Okuda K, Edwards CE, Martinez DR, et al. SARS-CoV-2 Reverse Genetics Reveals a Variable Infection Gradient in the Respiratory Tract. Cell **2020;** 182:429-46 e14.
33. Travaglini KJ, Nabhan AN, Penland L, Sinha R, et al. A molecular cell atlas of the human lung from single cell RNA sequencing. bioRxiv **2020**.
34. Wang C, Xie J, Zhao L, Fei X, et al. Alveolar macrophage dysfunction and cytokine storm in the pathogenesis of two severe COVID-19 patients. EBioMedicine **2020;** 57:102833.
35. Martines RB, Ritter JM, Matkovic E, Gary J, et al. Pathology and Pathogenesis of SARS-CoV-2 Associated with Fatal Coronavirus Disease, United States. Emerg Infect Dis **2020;** 26:2005-15.
36. Russell CD, Unger SA, Walton M, Schwarze J. The Human Immune Response to Respiratory Syncytial Virus Infection. Clin Microbiol Rev **2017;** 30:481-502.
37. Middleton EA, He XY, Denorme F, Campbell RA, et al. Neutrophil Extracellular Traps (NETs) Contribute to Immunothrombosis in COVID-19 Acute Respiratory Distress Syndrome. Blood **2020**.
38. Park MD. Macrophages: a Trojan horse in COVID-19? Nat Rev Immunol **2020;** 20:351.
39. Qin C, Zhou L, Hu Z, Zhang S, et al. Dysregulation of Immune Response in Patients With Coronavirus 2019 (COVID-19) in Wuhan, China. Clin Infect Dis **2020;** 71:762-8.
40. Liu Z, Long W, Tu M, Chen S, et al. Lymphocyte subset (CD4+, CD8+) counts reflect the severity of infection and predict the clinical outcomes in patients with COVID-19. J Infect **2020;** 81:318-56.
41. De Biasi S, Meschiari M, Gibellini L, Bellinazzi C, et al. Marked T cell activation, senescence, exhaustion and skewing towards TH17 in patients with COVID-19 pneumonia. Nat Commun **2020;** 11:3434.
42. Jiang Y, Wei X, Guan J, Qin S, et al. COVID-19 pneumonia: CD8(+) T and NK cells are decreased in number but compensatory increased in cytotoxic potential. Clin Immunol **2020;** 218:108516.
43. Files JK, Boppana S, Perez MD, Sarkar S, et al. Sustained cellular immune dysregulation in individuals recovering from SARS-CoV-2 infection. J Clin Invest **2021;** 131.

FIGURE LEGENDS

Figure 1. Representative hematoxylin-eosin (H&E) and immunohistochemistry (IHC) staining images of SARS-CoV-2 proteins, viral entry receptor ACE2 and markers of immune cells in lung tissues from COVID-19 patients. *A,* H&E images illustrating significant areas of lung tissues (case 2 in left images and case 4 in right images). An image of case 2 showing lung parenchyma with hemorrhagic infarct in top image (100x). A Langhans giant cell is visible in bottom image (asterisk, 600x). An image of case 4 with an early exudative phase of DAD, vascular congestion and rare hyaline membranes in top image (black arrow, 100x), and infiltrations of lymphocytes (white arrow) and macrophages (red arrow) in bottom image (600x). *B,* IHC detection of SARS-CoV-2 infection using antibody against spike protein (receptor binding domain, RBD) and NC protein (100x, case 2 in left images and case 4 in right images). A macrophage stained positive for S1 protein is visible in case 2 bottom image (black arrow, 600x). Case 2 has fewer positive cells compared to case 4 for both viral proteins. *C,* IHC detection of ACE2 protein expression in lung tissues (case 2 in left images and case 4 in right images). Immune cells identified in case 2 in bottom image are a monocyte (black arrowhead), a macrophage (black arrow) and a neutrophil (red arrowhead), all expressing ACE2 protein (600x). *D,* IHC detection of markers of immune cells in a lung tissue from a COVID-19 patient (case 3) consisting of monocytes and macrophages ($CD68^+$ and $CD163^+$), B cells ($CD19^+$ and $CD20^+$), different markers of T cells including T cell receptor ($CD3\varepsilon^+$), T regulatory cell (FOXP3), helper T cell ($CD4^+$), cytotoxic T cell ($CD8^+$), and lymphocyte common antigen ($CD45^+$) (100x).

Figure 2. Representative images of multicolor immunofluorescence staining of ACE2, SARS-CoV-2 proteins and cellular markers in lung tissues from COVID-19 patients. *A,* ACE2 protein (pseudo color red) and SARS-CoV-2 S1 protein (RBD, pseudo color green) in case 4. *B,* Alveolar epithelial type II / pneumocytes type II cells (AT2) (pseudo color green), ACE2 (pseudo color red) and SARS-CoV-2 S1 protein (RBD, pseudo color white) in case 5. *C,* Tyr-α-tubulin (pseudo color red) and SARS-CoV-2 NC protein (pseudo color green) in case 5. *D,*

MUC5AC (goblet cells, pseudo color green), ACE2 (pseudo color red) and SARS-CoV-2 S1 protein (RBD, pseudo color white) in case 4. *E,* MUC5B (club-like cells, pseudo color green), ACE2 (red) and SARS-CoV-2 S1 protein (RBD, pseudo color white) in case 4. *F,* CD34 (pseudo color green), ACE2 (red) and SARS-CoV-2 NC protein (pseudo color white) in case 5. *G,* CD31 (pseudo color red) and SARS-CoV-2 NC protein (pseudo color green) in case 1. Nuclei were stained with DAPI (pseudo color blue). Scale bar represents 20 μm.

Figure 3. Representative images of multicolor immunofluorescence staining of ACE2, SARS-CoV-2 S1 protein (RBD) and markers of innate immune response cells in lung tissues from COVID-19 patients. *A,* CD68, a monocytic lineage marker (pseudo color green), ACE2 (pseudo color red) and S1 protein (pseudo color white) in case 4. *B,* CD163, a macrophage M2 marker (pseudo color green), ACE2 (pseudo color red) and S1 protein (pseudo color white) in case 5. *C,* Elastase 2 (ELA-2), a neutrophil marker (pseudo color green), ACE2 (pseudo color red) and S1 protein (pseudo color white) in case 4. *D,* CD56, a NK cell marker (pseudo color red) and S1 protein (pseudo color green) in case 5. For *A* to *D*, nuclei were stained with DAPI (pseudo color blue). Scale bar represents 20 μm. *E,* Quantification of $CD68^+$, $CD163^+$, $ELA\text{-}2^+$ and $CD56^+$ cells in five different fields in each lung sample from all COVID-19 cases (Supplementary Figure 9). S1-positive and/or $ACE2^+$ cells were counted in the same fields and shown as percentages of positive cells. Statistical significance was determined using one-way analysis of variance (ANOVA) and Tukey's test for post hoc analysis. P values indicated when $p < 0.05$.

Figure 4. Representative images of multicolor immunofluorescence staining of ACE2, SARS-CoV-2 NC protein, and markers of B or T cells in lung tissues from COVID-19 patients. *A,* CD20, a B cell marker (pseudo color green), ACE2 (pseudo color red) and NC protein (pseudo color white) in case 5. *B,* CD4, a T helper cell marker (pseudo color green),

ACE2 (pseudo color red) and NC protein (pseudo color white) in case 1. *C,* CD8, a cytotoxic T cell marker (pseudo color green), ACE2 (pseudo color red) and NC protein (pseudo color white) in case 1. *D,* CD3ε, a T cell receptor marker (pseudo color green), ACE2 (pseudo color red) and NC protein (pseudo color white) in case 1. *E,* HLA-DR, a B and T cell activation marker (pseudo color green), ACE2 (pseudo color red) and NC protein (pseudo color white) in case 2. For *A* to *E*, nuclei were stained with DAPI (pseudo color blue). Scale bar represents 20 μm. *F,* Quantification of $CD20^+$, $CD4^+$, $CD8^+$, $CD3\varepsilon^+$ and $HLA\text{-}DR^+$ cells in five different fields in each lung sample from all COVID-19 cases (Supplementary Figure 10, 11). NC-positive and/or $ACE2^+$ cells were counted in the same fields and shown as percentages of positive cells. Statistical significance was determined using one-way analysis of variance (ANOVA) and Tukey's test for post hoc analysis. P values indicated when $p < 0.05$.

Figure 5. Representative images of multicolor immunofluorescence staining of IL6, SARS-CoV-2 S1 protein (RBD), and representative cellular markers in lung tissues from COVID-19 patients. *A,* IL6 (pseudo color red) and S1 protein (pseudo color green) in case 4. *B,* IL6 (pseudo color green), and cellular markers CD20 (pseudo color red), CD68 (pseudo color red) or CD163 (pseudo color red) in case 1. Nuclei were stained with DAPI (pseudo color blue). Scale bar represents 20 μm.

Table 1. Pertinent clinical-pathologic findings of the 5 studied COVID-19 cases

Case	Age* (years)	Sex	Underlying Conditions	Symptom Onset to Death	Clinical, Laboratory & Radiology	Final Anatomic Diagnosis and Post-Mortem CardioPulmonary Findings
1	50s	M	Hypertension, hyperlipidemia, nasal allergies	20 days	Hypoxemia (improved with supplemental O_2) CXR: patchy opacities NP NAAT: + SARS-CoV-2, Ct = 26.71 ↑ ferritin (maximum =1.9 x ref.) ↑ CRP (maximum = 22 x ref.) Rx: hydroxychloroquine; antibiotics (ceftriaxone/azithromycin →vancomycin/cefepime); heparin SC	PMI = 33 hrs FAD: Pulmonary thrombo-embolism, occluding right & left main pulmonary arteries, deep venous thrombosis, COVID-19 pneumonia Lungs - Massive pulmonary emboli, bilateral pulmonary consolidation, DAD. Hypertensive and atherosclerotic heart disease – cardiomegaly with left ventricular hypertrophy and coronary atherosclerosis
2	40s	M	Hypertension, HIV, asthma	10 days	Hypoxemia (required intubation) CXR: multiple bilateral opacities, NP NAAT: +SARS-CoV-2, Ct = 22.62 ↑ ferritin (maximum = 3.7 x ref.) ↑ CRP (maximum = 95.6 x ref) IL-6 (maximum = 16.4 x ref) Rx: hydroxychloroquine; antibiotics (ceftriaxone/azithromycin/vancomycin), hydrocortisone IV, enoxaparin SC	PMI =16 hrs FAD: Pulmonary thrombo-embolism, occluding right main pulmonary artery, deep venous thrombosis, COVID-19 pneumonia, hypertensive cardiovascular disease Lungs - Massive pulmonary emboli, bilateral pulmonary

						consolidation, DAD. Hypertensive heart disease – cardiomegaly with left ventricular hypertrophy
3	30s	M	Hypertension	13 days	Hypoxemia (required intubation) CXR: bilateral patchy infiltrates NP NAAT: + SARS-CoV-2, Ct = 36.50 ↑ ferritin (maximum =7.4 x ref.) ↑ CRP (maximum = 40.9 x ref.) ↑ D-dimer (maximum = 1.5 x ref) ↑ Il-6 (maximum = 4.4 x ref) Rx: hydroxychloroquine; antibiotics (ceftriaxone/azithromycin →cefepime); enoxaparin SC	PMI = 7 hrs FAD: COVID-19 pneumonia, hypertensive and atherosclerotic cardiovascular disease Lungs - Bilateral pulmonary consolidation, DAD. Hypertensive and atherosclerotic heart disease - cardiomegaly and coronary atherosclerosis
4	70s	M	Parkinson's Disease, hyperlipidemia	11 Days	Hypoxemia (refused intubation) CXR: Left lower lobe consolidation, right basilar and bilateral mid-lung patchy opacities NP NAAT: +SARS-CoV-2, Ct= 18.34 ↑ ferritin (maximum = 7.1 x ref) ↑ CRP (maximum = 38 x ref) ↑ D-dimer (maximum = 11.7 x ref) Rx: hydroxychloroquine; antibiotics (vancomycin/cefepime); heparin SC→enoxaparin SC	PMI = 59 hrs FAD: Acute pneumonia, SARS-CoV-2, Parkinson's Disease Lungs - Bilateral pulmonary congestion & consolidation, DAD and focal superimposed acute pneumonia. Cardiomegaly
5	50s	F	Stage 4 chronic kidney disease	9 days	Hypoxemia (refused intubation), Diarrhea CXR: Multiple bilateral ground-glass opacities NP NAAT: +SARS-CoV-2, Ct = 33.37 ↑ ferritin (maximum= 8.7 x ref) ↑ CRP (maximum = 71 x ref) ↑ D-dimer (maximum = 26.2 x ref) ↑ procalcitonin (maximum = 15.3 x ref)	PMI = 4 hrs FAD: COVID-19 pneumonia, hypertensive cardiovascular disease, End stage renal disease Lungs – congestion and possible consolidation,

					↑ Il-6 (maximum = 56.8 x ref) ↑ IL-8 (maximum = 16.9 x ref) ↑ TNFα (maximum = 1.6 x ref) Rx: hydroxychloroquine; antibiotics (ceftriaxone/azithromycin); enoxaparin SC → heparin SC	DAD. Cardiomegaly

* No specific age is given to avoid identification of subject. M: male, F: female, CXR: chest radiograph, NP: nasopharyngeal, NAAT: nucleic acid amplification test, Ct: Cycle threshold (averaged), CRP: C-reactive protein, ref.: upper reference range, IL: interleukin, TNF-α: Tumor necrosis factor-alpha, PMI: post-mortem interval, FAD: Final anatomic diagnosis, DAD: diffuse alveolar disease.

Figure 1

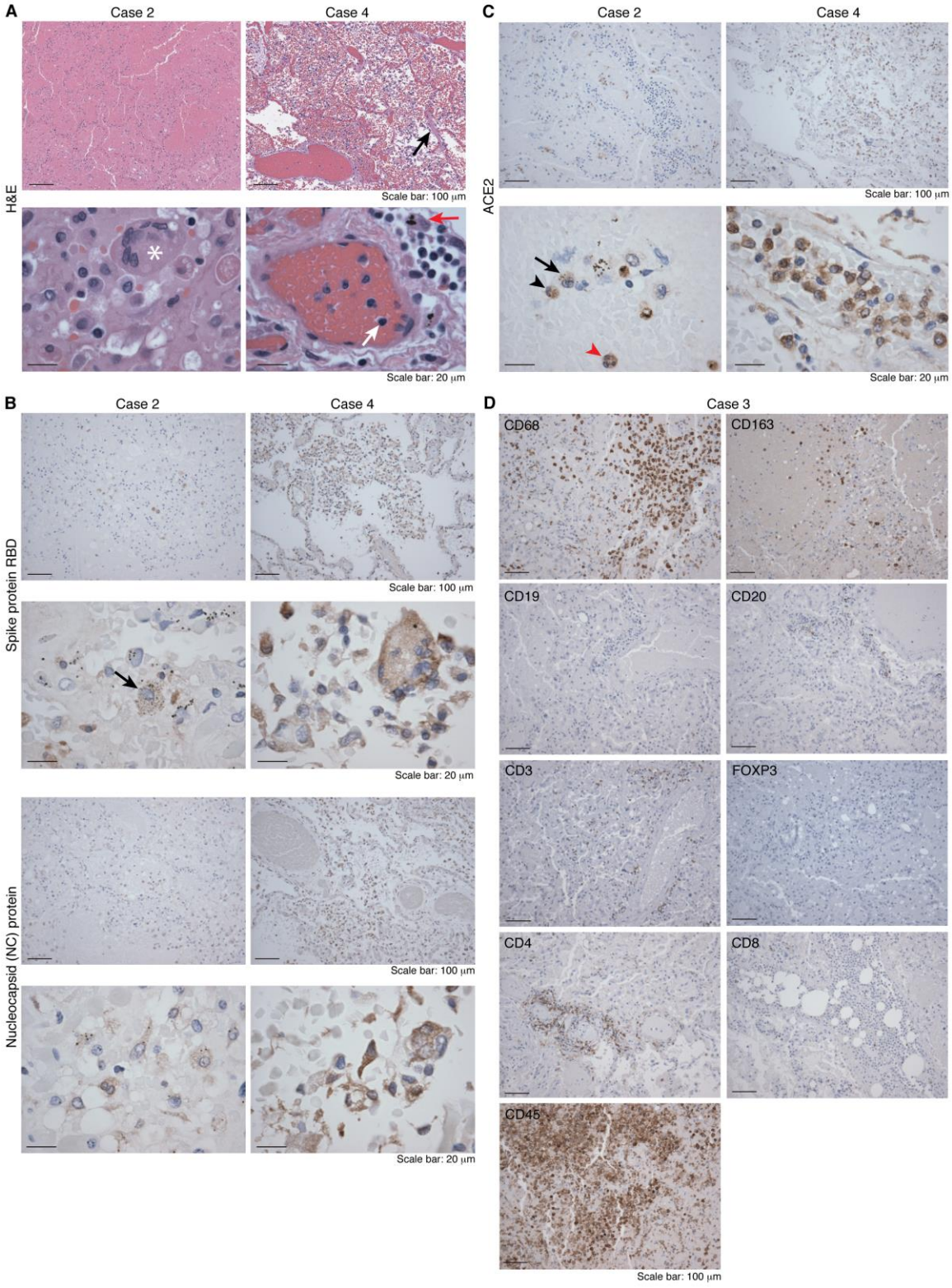
A
Case 2
Case 4
H&E
Scale bar: 100 μm
Scale bar: 20 μm
C
Case 2
Case 4
ACE2
Scale bar: 100 μm
Scale bar: 20 μm
B
Case 2
Case 4
Spike protein RBD
Scale bar: 100 μm
Scale bar: 20 μm
Nucleocapsid (NC) protein
Scale bar: 100 μm
Scale bar: 20 μm
D
Case 3
CD68
CD163
CD19
CD20
CD3
FOXP3
CD4
CD8
CD45
Scale bar: 100 μm

Figure 2

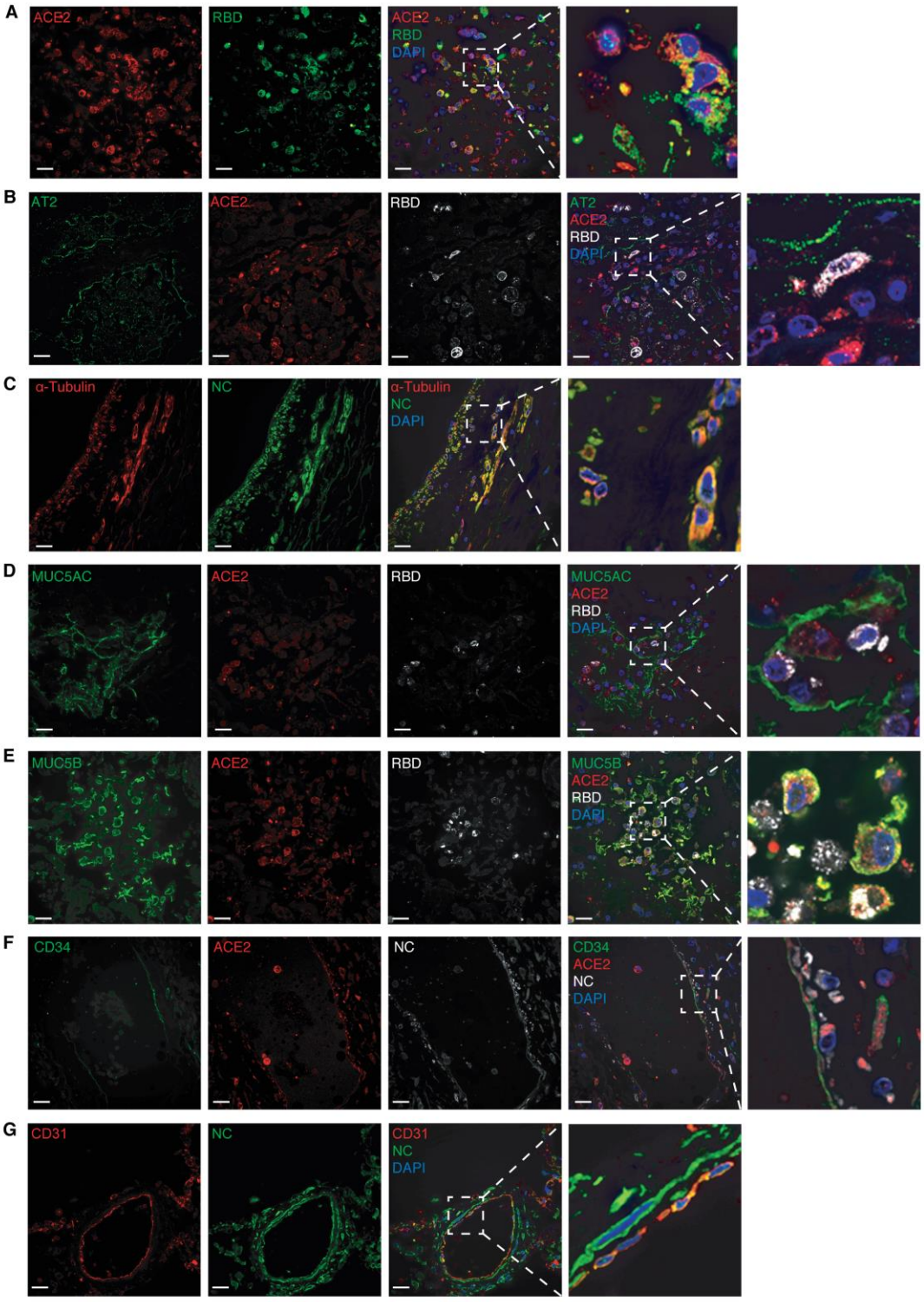
A
ACE2
RBD
ACE2
RBD
DAPI
B
AT2
ACE2
RBD
AT2
ACE2
RBD
DAPI
C
α-Tubulin
NC
α-Tubulin
NC
DAPI
D
MUC5AC
ACE2
RBD
MUC5AC
ACE2
RBD
DAPI
E
MUC5B
ACE2
RBD
MUC5B
ACE2
RBD
DAPI
F
CD34
ACE2
NC
CD34
ACE2
NC
DAPI
G
CD31
NC
CD31
NC
DAPI

Figure 3

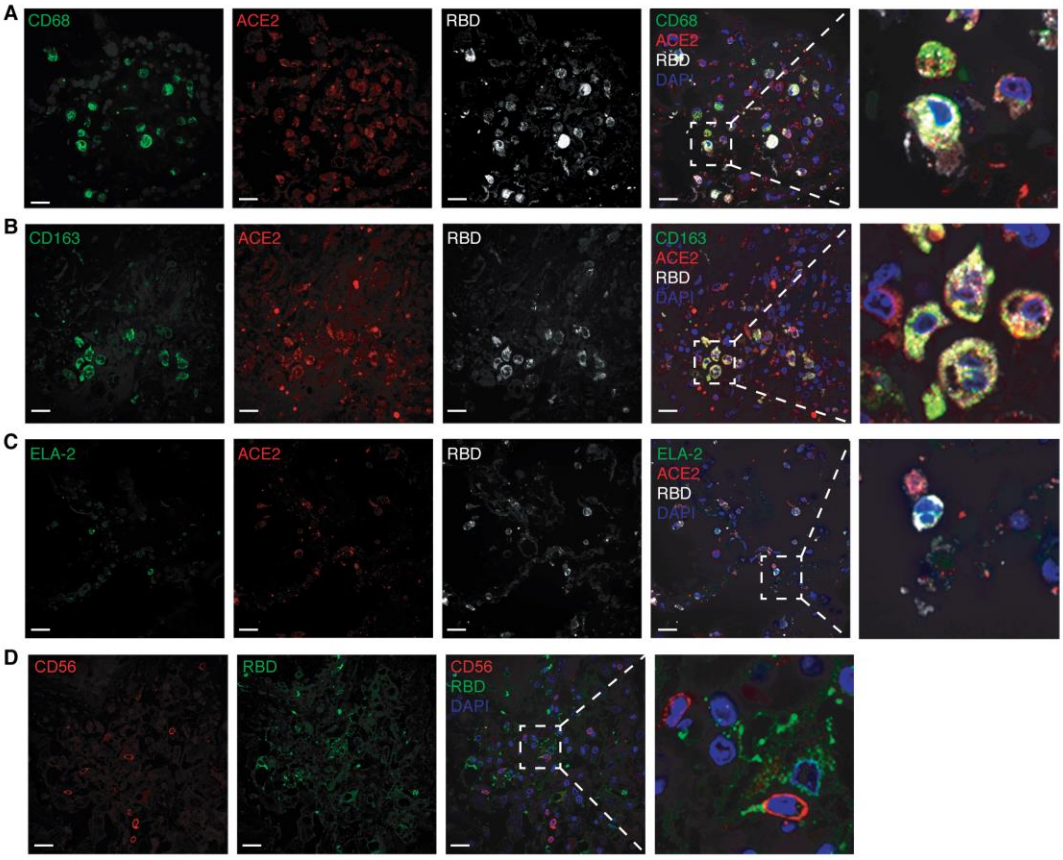
A
CD68
ACE2
RBD
CD68
ACE2
RBD
DAPI
B
CD163
ACE2
RBD
CD163
ACE2
RBD
DAPI
C
ELA-2
ACE2
RBD
ELA-2
ACE2
RBD
DAPI
D
CD56
RBD
CD56
RBD
DAPI

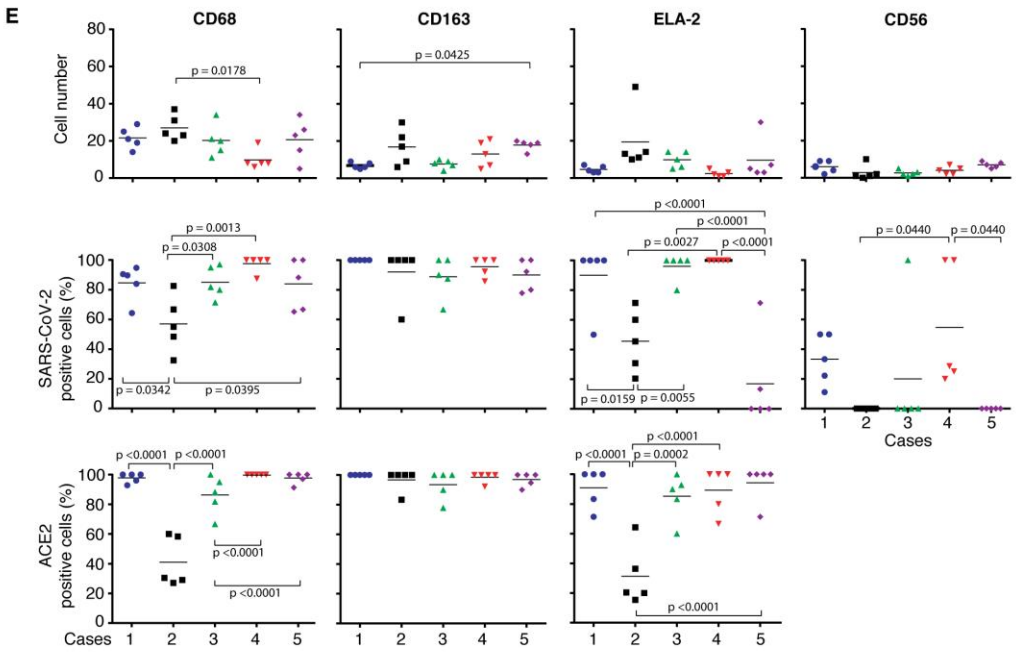
E
CD68
CD163
ELA-2
CD56
Cell number
p = 0.0178
p = 0.0425
SARS-CoV-2 positive cells (%)
p = 0.0013
p = 0.0308
p = 0.0342
p = 0.0395
p <0.0001
p <0.0001
p = 0.0027
p <0.0001
p = 0.0159
p = 0.0055
p = 0.0440
p = 0.0440
ACE2 positive cells (%)
p <0.0001
p <0.0001
p <0.0001
p <0.0001
p <0.0001
p <0.0001
p = 0.0002
p <0.0001
Cases
1
2
3
4
5

Figure 4

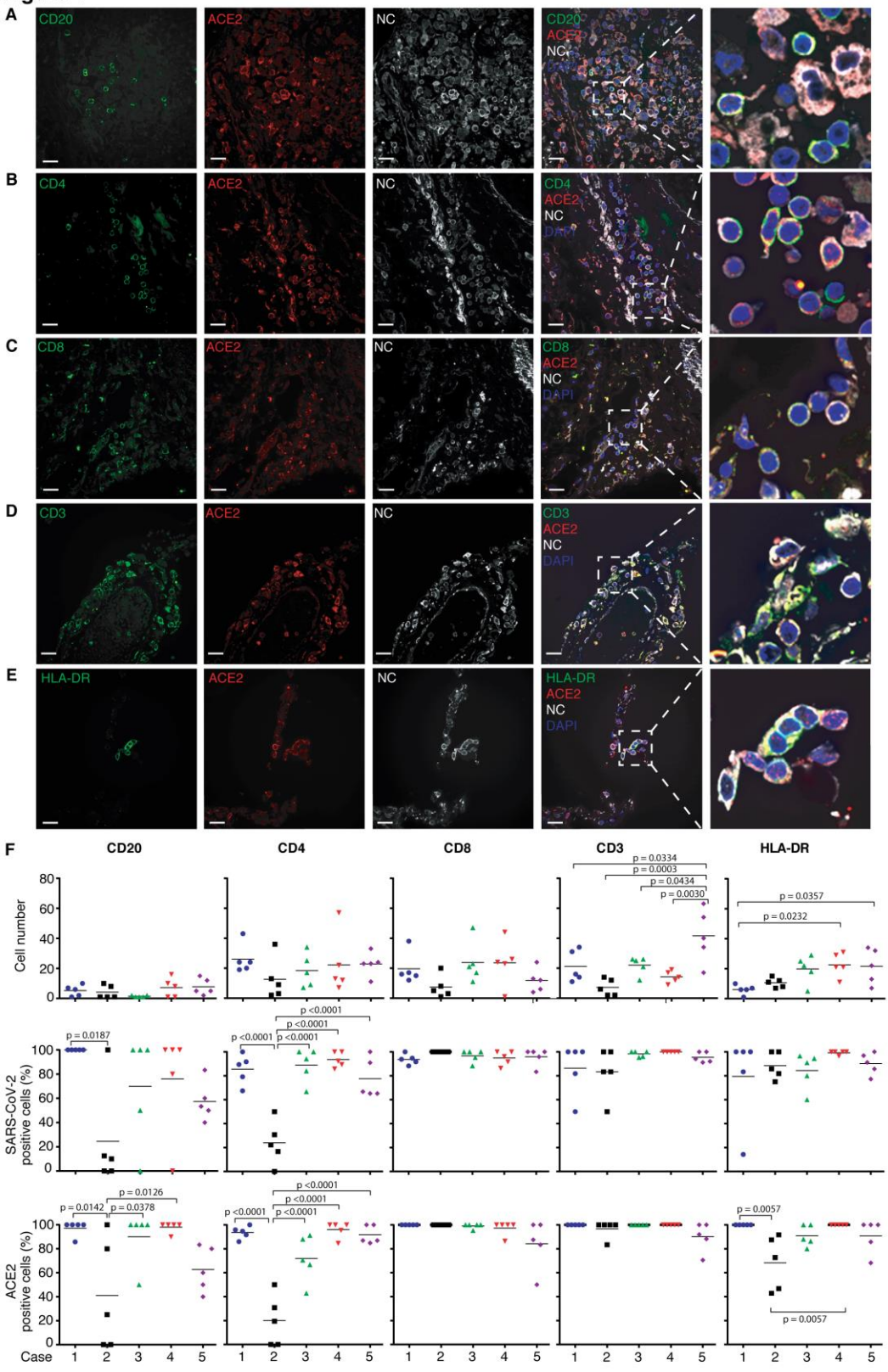
A
CD20
ACE2
NC
CD20
ACE2
NC
B
CD4
ACE2
NC
CD4
ACE2
NC
DAPI
C
CD8
ACE2
NC
CD8
ACE2
NC
DAPI
D
CD3
ACE2
NC
CD3
ACE2
NC
DAPI
E
HLA-DR
ACE2
NC
HLA-DR
ACE2
NC
DAPI
F
CD20
CD4
CD8
CD3
HLA-DR
Cell number
SARS-CoV-2 positive cells (%)
ACE2 positive cells (%)
Case
p = 0.0187
p = 0.0142
p = 0.0378
p = 0.0126
p <0.0001
p = 0.0334
p = 0.0003
p = 0.0434
p = 0.0030
p = 0.0357
p = 0.0232
p = 0.0057

Figure 5

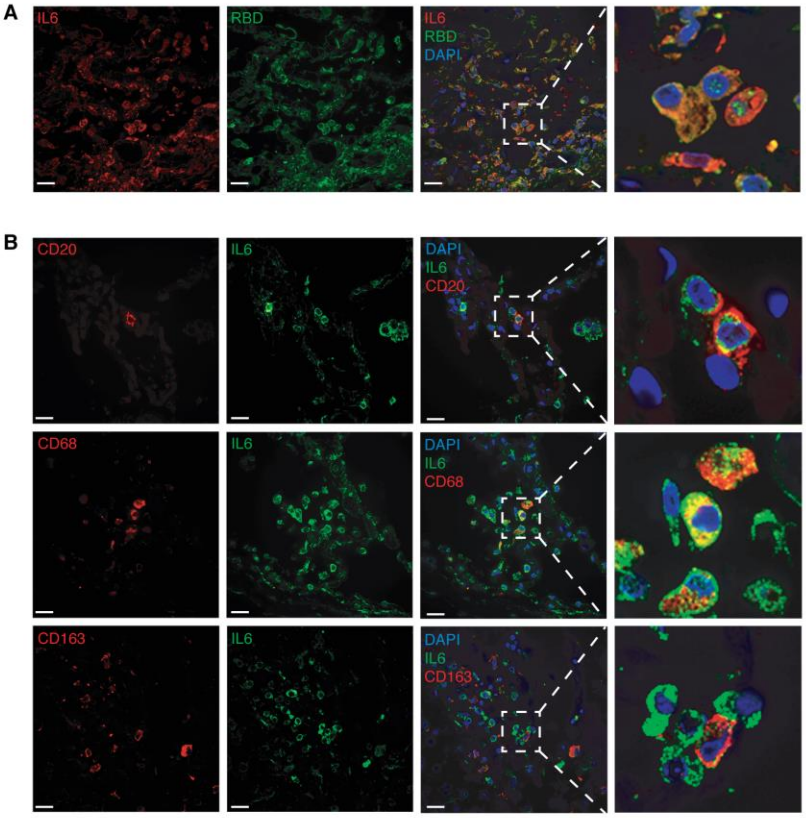
A
IL6
RBD
IL6
RBD
DAPI
B
CD20
IL6
DAPI
IL6
CD20
CD68
IL6
DAPI
IL6
CD68
CD163
IL6
DAPI
IL6
CD163